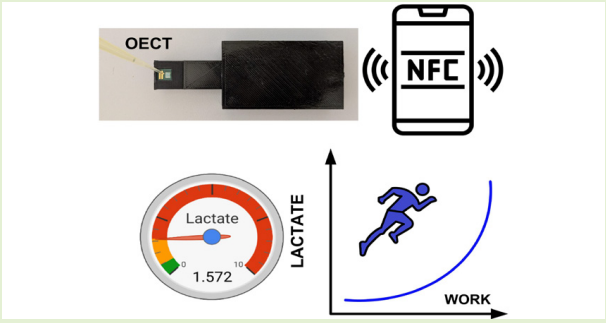
Near-Field Communications Sensor for Lactate Determination in Saliva and Sweat Using Organic Electrochemical Transistors (OECTs)

Antonio Lazaro, *Senior Member, IEEE*, Emma Rojas Rodriguez, Marc Lazaro, Ramon Villarino, Benito González, and David Girbau, *Senior Member, IEEE*

***Abstract*—Organic electrochemical transistors (OECTs) are attractive devices for the next generation of biosensors, but their widespread adoption has been limited by the need for expensive and bulky measurement instruments. This work addresses this limitation by presenting a low-cost, low-power readout circuit for biasing and measuring the drain current of OECTs, specifically targeting portable and wearable applications for point-of-care testing (POCT). The proposed system utilizes a modified microcontroller-based potentiostat that is compatible with single positive voltage sources. It also includes near field communication (NFC), which allows data to be retrieved wirelessly using a smartphone. A proof-of-concept lactate sensor is presented, designed for measuring lactate concentration in sweat and saliva. The sensor is based on an OECT with a platinum-coated gate and a Nafion membrane that immobilizes the lactose oxidase enzyme, significantly improving the selectivity of the substance to be measured. Low detection limits of 0.35 and 0.0485 mM have been achieved in sweat and saliva, respectively. This research provides a complete, low-cost, and noninvasive solution for OECT-based biosensors.**



***Index Terms*— Biopotentiostat, biosensor, near-field communications (NFC), organic electrochemical transistors (OECTs), point-of-care testing (POCT).**

I. Introduction

LACTATE is a metabolite directly produced in its ionized form during glucose metabolism, which is predominantly composed of L-lactate, which is the physiologically more significant isomer. It is a byproduct of anaerobic metabolism, which occurs when the body produces energy without sufficient oxygen. Lactate is found not only in blood but also in other biofluids, including sweat, saliva, and interstitial fluid. Sweat lactate, which is produced in the muscle during exercise or other physical activity [1], and is dependent on individual motor function, has emerged as one of the most important biomarkers for assessing fatigue and excessive exercise [2]. When muscles consume oxygen faster than they receive it, they produce lactate as a temporary energy source. Interestingly, lactate can be recycled by the liver and converted back into glucose through a process called gluconeogenesis [3], providing a vital source of energy during strenuous activities. In addition, elevated lactate levels can be associated with several diseases such as lactic acidosis [4], sepsis and septic shocks [5], hypoxia that lead to low oxygen levels in the blood associated with pulmonary disorders or circulatory issues [6], liver and kidney dysfunctions [7], hemoglobin disorders [8], or intestinal ischemia [9]. Monitoring lactate concentration has aroused great interest in recent years. However, lactate measurement is typically conducted using blood samples, and real-time data acquisition systems are not yet commercially available. Indeed, other biological fluids such as sweat, saliva, and tears are easier to measure,

Received 17 September 2025; revised 12 December 2025; accepted 13 December 2025. Date of publication 22 December 2025; date of current version 2 February 2026. This work was supported by MICIU/AEI/10.13039/501100011033/ERDF, European Union (EU), under Project PID2021-122399OB-I00 and Project PID2024-1551730B-I00. The associate editor coordinating the review of this article and approving it for publication was Prof. Maryam Shojaei Baghini. *(Corresponding author: Antonio Lazaro.)*

Antonio Lazaro, Emma Rojas Rodriguez, Marc Lazaro, Ramon Villarino, and David Girbau are with the Electronics, Electrical and Automatics Engineering Department, Rovira and Virgili University, 43007 Tarragona, Spain (e-mail: antonioramon.lazaro@urv.cat; emmaaro16@gmail.com; marc.lazaro@urv.cat; ramon.villarino@urv.cat; david.girbau@urv.cat).

Benito González is with the Institute for Applied Microelectronics, Universidad de Las Palmas de Gran Canaria, Campus Universitario de Tafira, 35017 Las Palmas, Spain (e-mail: benito@iuma.ulpgc.es).

Digital Object Identifier 10.1109/JSEN.2025.3645137

© 2025 The Authors. This work is licensed under a Creative Commons Attribution 4.0 License.
For more information, see https://creativecommons.org/licenses/by/4.0/

making them attractive targets for noninvasive or minimally invasive portable sensing platforms [10]. Furthermore, recent studies have reported several quantitative correlations between biomarker levels in blood and those in sweat or saliva [1], [11], [12], [13], [14], highlighting the medical relevance of these biofluids. Although some sweat sensors are currently under development [1] to address market demand, they have not yet reached widespread use. Wearable chemical sensors for continuous real-time monitoring of sweat composition are a very attractive concept for sports performance, as they allow physiological information to be obtained without disturbing athletes during exercise [15], [16]. During intense physical activity, the working muscles may experience an unwanted build-up of lactate, leading to soreness, pain, and fatigue [17]. Consequently, monitoring changes in blood lactate concentration is a common practice to assess endurance in elite athletes, often using the well-known threshold curve [18], [19]. Understanding blood lactate levels is crucial for runners as it provides insight into the metabolic demands of their training and performance. A lactate curve, also known as a lactate profile or lactate threshold curve, is a graphical representation that illustrates the relationship between work intensity and blood lactate levels (see Fig. 1). It is a tool used to analyze the body's response to increased exercise intensity. There are two key thresholds: the lactate threshold or aerobic threshold. This is the point at which lactate levels begin to rise significantly, starting to increase noticeably but moderately, becoming a transitional stage from aerobic to anaerobic energy production. It is associated with moderate exercise intensity and can be sustained for a long time. Second is lactate threshold, or maximal lactate steady state (MLSS). It is the point at which lactate production exceeds the body's ability to eliminate it, leading to rapid accumulation. This is a higher intensity point where fatigue occurs more quickly. By identifying these thresholds, athletes can optimize their training. The goal is to "shift the lactate curve to the right," which means they can maintain a higher intensity of exercise before lactate accumulates, indicating greater endurance.

Organic electrochemical transistors (OECTs) are a type of organic thin film devices that have increasingly attracted attention for use in chemical and biological sensing applications. These devices have demonstrated sensing capabilities for ion [20], [21], [22], [23], pH [24], [25], glucose [26], [27], [28], lactate [29], dopamine [27], [30], and uric acid (UA) [31] detection among others.

Therefore, different substrates, including flexible materials and methods for developing wearable and portable sensors based on these transistors, have been reported in [32], [33], [34], and [35]. However, most of the results presented in the literature are obtained using expensive instruments such as source meaure unit (SMU). Few studies employ low-cost electronic devices for data readout, despite their importance for the development of practical commercial systems [36], [37]. On the contrary, the main novelty of this article is that it proposes a low-cost and low-power readout circuit for biasing and measuring the current in OECT for portable and wearable applications.

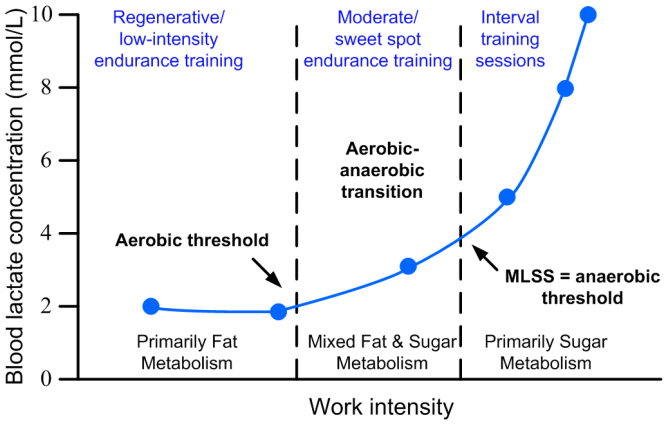


Fig. 1. Typical graph of lactate concentration versus work intensity. The three states associated with endurance training intensity are observed: aerobic (low intensity), aerobic-anaerobic transition (moderate intensity), and MLSS, or maximum lactate steady state (moderate intensity over long periods).

The article is organized as follows. Section II provides an overview of how the OECT works as a chemical sensor. The main blocks of the system are described in Section III. Section III-A details a low-cost OECT manufactured using standard PCB circuits, which is used in our tests. The functionalization of the gate for lactate detection is described in Section III-A2. In Section III-B, we propose a circuit for measuring the OECT current and describe a proof-of-concept sensor for detecting lactate in saliva and sweat with near-field communication (NFC) communication to a smartphone. Experimental results are presented in Section IV, followed by a comparison with other sensors in the same section. Finally, Section V provides the conclusion.

II. Background on OECT as a Chemical Sensor

The typical structure of an OECT, shown in Fig. 2(a), consists of three metallic electrodes: a source, a drain, and a gate. A channel made of a semiconducting polymer connects the source and the drain. Both the channel and the gate are immersed in an electrolyte. The most widely used polymer is the p-type conductive poly(3,4-ethylenedioxythiophene) doped with poly(styrene sulfonate) (PEDOT:PSS). When a source-drain voltage (V_{DS}) is applied, a drain current (I_{DS}) controlled by the gate voltage (V_{GS}) flows through the channel. By applying a positive gate voltage (V_{GS}), a transfer of cations to the PEDOT:PSS channel from the electrolyte occurs, causing a decrease in the concentrations of holes in the channel and, consequently, a reduction in the conductivity of the PEDOT. This will deplete the number of available carriers, and hence, the drain-source current decreases. The de-doping process in the channel is described by the following equation:

$$\mathrm{PEDOT^+ : PSS^- + M^+ + e^- \leftrightarrow PEDOT + M^+ : PSS^-} \quad (1)$$

where M^+ is the cation injected from the electrolyte. The threshold voltage (V_T) is defined as the gate voltage at which the channel is de-doped and the current flowing through it is

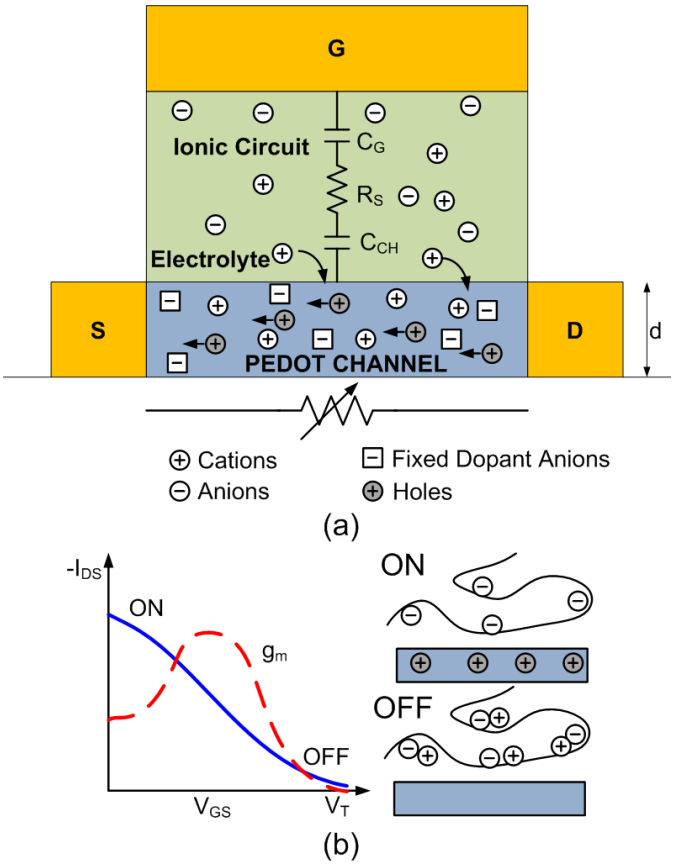


Fig. 2. (a) Diagram of an OECT, showing the source (S), drain (D), electrolyte, and gate (G). The equivalent circuit model of the electrolyte is a series RC, while the channel is modeled with a variable resistance controlled by the gate voltage. (b) Transfer curve showing the operation of an OECT with a conducting polymer channel. At zero gate voltage, holes in the conducting channel contribute to a high drain current, and the transistor turns on. When a gate voltage is applied, the holes are replaced by cations and the transistor turns off.

zero. For $V_{DS} < V_{GS} - V_T$, the transistor is in the linear region and the drain current is nearly linear with V_{DS}, whereas in the saturation region ($V_{DS} > V_{GS} - V_T$), the current is nearly independent of the drain voltage and is controlled by the gate voltage.

An important parameter in the operation of OECT is the transconductance (g_m), which is defined as the derivative of the channel current with respect to the gate voltage ($g_m = (dI_{DS})/(dV_{GS})$). A simplified model that describes the OECT drain current I_{DS} is reported by Daniel Bernards and George Malliaras [38]. Experimental results show that transconductance presents a peak that cannot be modeled with the simplified Bernards' model [39]. In a recent work [40], the authors have presented a novel model that solves this drawback based on the carrier density derived from the Nernst equation and an improved mobility model.

The equivalent capacitance of the device (C_{eq}) consists of two capacitors in series, one at the gate/electrolyte interface (C_G) and one at the electrolyte/channel interface (C_{CH}) (see Fig. 2). Therefore, the transconductance is proportional to μC_{eq}, and the response speed is proportional to $1/(R_S \cdot C_{eq})$, being μ the mobility and R_S is the solution resistance. The

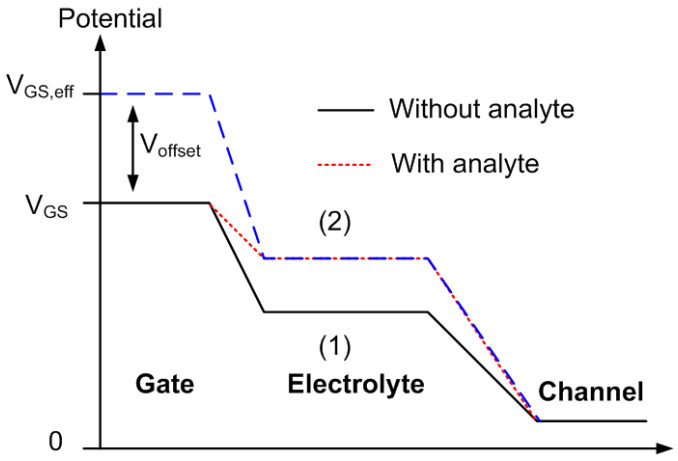


Fig. 3. Potential diagram of the OECT. In the absence of an analyte (solid line), the electrolyte potential (1) is determined by the relative capacitances at the gate and channel interfaces. In the presence of an analyte (dotted line), the electrolyte potential (2) is increased according to the Nernst equation. The effective gate voltage (dashed line) is that required to produce the same electrolyte potential (2) in the absence of Faradaic effects.

equivalent capacitance is therefore given by:

$$C_{eq} = \frac{1}{1/C_G + 1/C_{CH}}. \tag{2}$$

In many interesting applications, $C_G \gg C_{CH}$. In such cases, the contribution of the gate capacitance becomes negligible.

The addition of an analyte increases the electrolyte potential, reducing the channel current. Bernards et al. [26] defines the effective gate voltage $V_{GS,eff}$ as the voltage that would need to be applied to the gate electrode (in the absence of Faradic effects) to produce the same channel current (see Fig. 3). The effective gate voltage can be expressed as follows:

$$V_{GS,eff} = V_{GS} + V_{offset}. \tag{3}$$

This offset shift V_{offset} is described by the Nernst equation and scaled by the factor $(1 + \gamma)$, where γ is the capacitance ratio ($\gamma = C_{CH}/C_G$), and C_{CH} and C_G are the channel and gate capacitances, respectively,

$$V_{offset} = (1 + \gamma)\frac{kT}{ne}\ln\frac{[Ox]}{[Red]} \tag{4}$$

where [Ox] and [Red] are the concentrations of oxidized and reduced species, k is the Boltzmann constant, T is the temperature, e is the electron charge, and n is the number of electrons transferred during the reaction.

Transconductance is a key parameter, since the change in drain-to-source current due to the presence of the analyte is expressed as follows:

$$\Delta I_{DS} \approx g_m \cdot V_{offset}. \tag{5}$$

Therefore, to optimize sensitivity, the transistor should be biased in a region where the transconductance is high.

III. System Overview

A. Sensor Fabrication

1) OECT Manufacturing: A thick-film OCET was manufactured for the test. Standard PCB substrates such as

FR4 or flexible polyamide (Kapton) were used. The source, drain, and gate electrodes and the interconnections have been manufactured using standard PCB techniques. To protect the Cu electrodes from corrosion, an ENIG (electroless nickel immersion gold) surface finish was applied, consisting of a two-layer metallic surface finish that included a thin layer of gold (2 μm) over a layer of nickel. Thickness of metallization is 35μm. A layer of insulating resin is used to protect the interconnections, leaving only the electrodes exposed.

The gate is coated with a layer of approximately 1 μm by electroplating with a platinum solution provided by SPA PLATING (U.K.).

A 3%–4% aqueous solution of high-conductivity-grade poly (3,4-ethylenedioxythiophene): poly(styrene sulfonate) (PEDOT:PSS) was used to manufacture the channel. The PEDOT:PSS was purchased from Sigma-Aldrich (Reference 655201-25G). The gate electrode is protected with a tape that leaves only the channel region visible. The PEDOT is deposited onto the channel by spinning at 1500 r/min for 30 s. It is then cured at 100 °C for a 20 min in an oven. Finally, the tape is removed, and the board is cleaned with water.

Once the channel cools to room temperature, it is immersed for 2 h in a 10^{-2} M KCl solution with constant stirring. Finally, the system was rinsed three times with distilled water for 5 min.

2) Gate Functionalization: The final step of the fabrication is the functionalization of the gate with the enzyme and its immobilization. The LOx enzyme is commonly employed as a selective catalyst to convert L-lactate into pyruvate in the presence of molecular oxygen [41], [42]

$$\mathrm{L-lactate} + \mathrm{O_2} \xrightarrow{\mathrm{LOx}} \mathrm{pyruvate} + \mathrm{H_2O_2}. \tag{6}$$

By applying a certain electrical voltage, hydrogen peroxide can be oxidized on a Pt surface (gate electrode)

$$\mathrm{H_2O_2} + \mathrm{O_2} \xrightarrow{Pt} 2\mathrm{H^+} + \mathrm{O_2} + 2\mathrm{e^-}. \tag{7}$$

The oxidation of L-lactate produces a change in the effective gate voltage according to the Nernst equation that depends on the concentration.

The steps for preparing the gate electrodes are as follows.

1) *Electrode Preparation:* After cleaning, the gate electrode was coated with a layer of electrodeposited Pt.
2) *Enzyme Immobilization:* Lactate oxidase (>20 U/mg Iyophilized powder) was provided by Sigma-Aldrich (Reference L9795). A solution containing 10 mg/mL of LOx in 0.1 M phosphate-buffered saline (PBS) was prepared. Any solution not immediately used for sensor preparation was stored at 4 °C for up to 24 h. Nafion (a sulfonated tetrafluoroethylene-based fluoropolymer-copolymer) was used for the immobilization of the enzyme LOx. For this purpose, a first layer of Nafion was deposited on the Pt gate by applying a diluted solution of Nafion (5 wt. % in a mixture of lower aliphatic alcohols and water). After drying the Naphion layer for 1 h at room temperature, 3 μL of the enzyme solution was applied to the gate and left to dry for approximately 60 min.

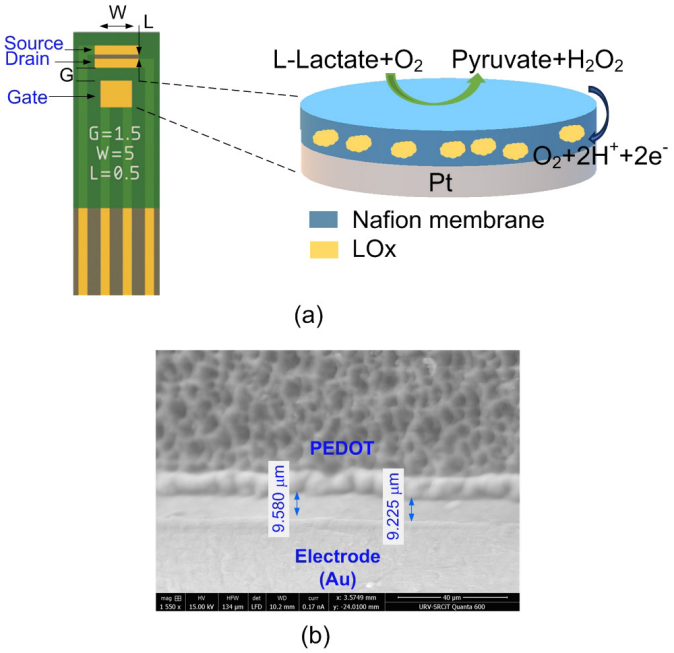


Fig. 4. (a) Image of the manufactured coplanar OECT and detail of the Nafion membrane with the enzyme LOx on the gate. (b) SEM image of the channel indicating the distance from the edge of the electrode.

3) *Nafion Coating:* Another layer of Nafion solution is then added. The resulting Nafion film stabilizes the enzyme layer on the electrode surface, which improves the durability of the sensor. It also helps to preserve enzyme activity by preventing leaching. Sensors were stored in 0.1 M PBS solution (Sigma-Aldrich, P3813) at 4 °C until use.

In addition, Nafion acts as a selective barrier that minimizes interference from substances present in complex biological matrices, such as blood, saliva, or sweat. It has a negative charge, which allows the transport of protons (H^+), while repelling interference with identical charges (e.g., ascorbate, urate).

Fig. 4 shows the structure of the OECT and a SEM image of the channel. The width (W), thickness (d), and length (L) of the channel are 5 mm, 25.5 μm, and 0.5 mm, respectively. The gold source/drain terminals are 5 × 1 mm^2, and a 10.5 mm^2 gate electrode was used. The separation between the drain and gate electrodes (G) is 1.5 mm. The channel thickness, d, is estimated by comparing it with the thickness of the electrode metallization (35 μm).

B. NFC-Based Platform

The characterization of the drain current in OECT-based biosensors is often performed using a SMU with two outputs. These instruments can apply arbitrarily positive or negative voltages while measuring the current through the terminals. However, these instruments are not suitable for low-cost and low-volume applications such as point-of-care testing (POCT) or small laboratories. In the case of P-channel OECTs (such as those based on PEDOT), negative voltages must be applied between the drain and the source. This negative voltage must be generated from positive batteries in the

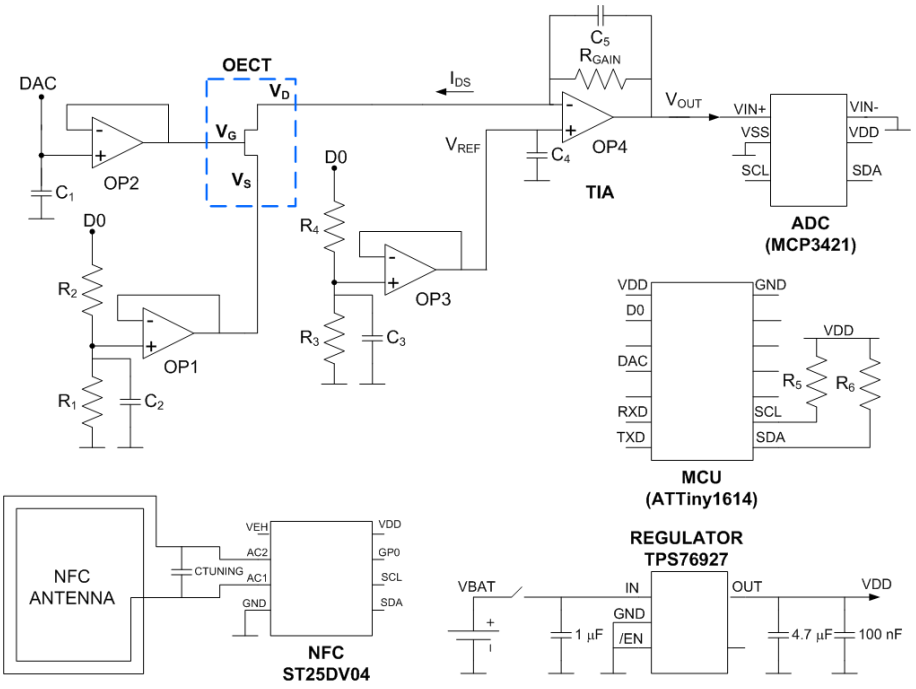


Fig. 5. AFE diagram.

case of POCT. To achieve this, two batteries are needed, or alternatively, a switching inverter regulator must be used, which introduces switching-related noise [43]. This work proposes an analog front-end (AFE) based on a modified dual-channel potentiostat, which is compatible with single positive voltage sources and microcontrollers. It should be noted that in another work [43], a NFC-based device was proposed, in which the drain current was measured from the voltage drop across a series resistor at the drain electrode. Consequently, the drain-to-source voltage depended on the measured current, in contrast to the constant voltage provided by the AFE proposed in this work. The circuit schematic is shown in Fig. 5.

In this work, the front-end consists of a low-power microcontroller with a digital-to-analog output (DAC) and a potentiostat that allows the gate and drain-to-source voltages to be set, respectively. The current I_{DS} can be obtained thanks to a transimpedance amplifier (TIA), whose output voltage is measured with an analog-to-digital converter (ADC). Microchip's low-power Attiny1614 microcontroller features an 8-bit DAC and a 10-bit ADC. The Attiny1614 microcontroller from Microchip is a low-power 8-bit microcontroller with a 10-bit DAC. Therefore, in this work, it is not necessary to use an external DAC. However, since the drain current can vary by several orders of magnitude, an external ADC can provide more bits and less noise than the microcontroller's internal ADC. The ADC MCP3421 from Microchip is used in this work. This IC is a sigma-delta converter with 18 bit at 3.75 samples per second (SPS) and 16 bits at 15 SPS. The MCP3421 ADC performs the conversion at rates of 3.75, 15, 60, or 240 SPS depending on the bit configuration defined by the user via the two-wire I2C serial interface. At 3 V, the ADC draws only 145 μA. Usually, in biosensors, the drain current is measured by sweeping the gate voltage and maintaining a fixed V_{DS} or at a fixed gate voltage, such as in the case of chronoamperometry, where the current is recorded as a function of time. Therefore, to avoid the need for a second DAC, the drain voltage, which comes from voltage dividers enabled by a microcontroller output signal, is kept fixed

$$V_{DS} = V_{REF} - V_S \tag{8}$$

where

$$V_S = \frac{R_1}{R_1 + R_2} V_{DD} \tag{9}$$

$$V_{REF} = \frac{R_3}{R_3 + R_4} V_{DD}. \tag{10}$$

Typically, the value of V_S is 1 V, so that from (9) the appropriate resistor values for the divider are selected. On the other hand, V_{REF} is adjusted according to (10) to obtain the desired drain voltage. The gate voltage is programmable using the microcontroller's internal DAC. To avoid any loading effects, operational amplifiers configured as voltage followers were used. The drain-to-source current is obtained from the gain of the TIA implemented with the operational amplifier OP4

$$I_{DS} = -\frac{V_{OUT} - V_{REF}}{R_{GAIN}}. \tag{11}$$

The LMV358 low-cost dual rail-to-rail operational amplifier from Texas Instruments has been selected for the implementation of voltage followers and the TIA. Optimized for low-voltage, battery-powered systems, it operates at 2.7 V with a low quiescent current of 140 μA, a typical input offset voltage of 1 mV, an input bias current of 45 nA, and a unit-gain bandwidth of 1 MHz.

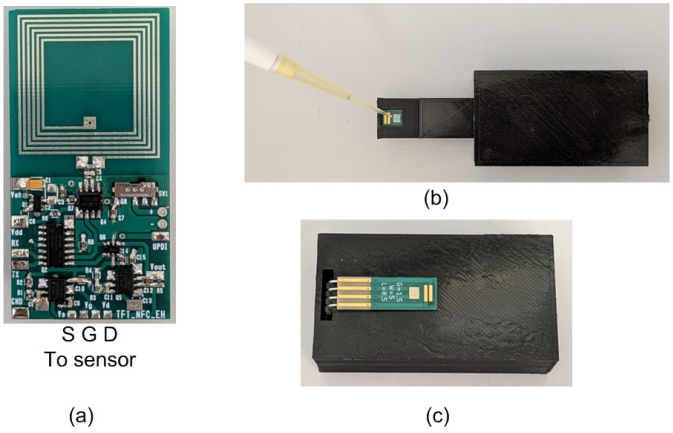


Fig. 6. (a) Manufactured board. (b) Prototype of lactate sensor for saliva. (c) Prototype of lactate sensor for sweat monitoring.

NFC was used to retrieve the data. An ST25DV04 NFC IC was selected for this purpose. Data are stored in the IC's internal EEPROM via the I^2C bus. A scaled version of the antenna described in [44] was used in this work. A 25 × 25 square coil antenna with 0.5 mm wide traces and 6 turns was used. The inductance of the antenna is 1.67 μH, and the resonance frequency of the tag was tuned with a 60 pF tuning capacitor to 13.56 MHz following the procedure described in [44] and [45]. A photograph of the manufactured board is shown in Fig. 6(a). The prototype dimensions are 3 × 5 cm. A proof of concept lactate sensor for saliva and sweat is shown in Fig. 6(b) and (c), respectively. In the case of the sweat sensor, the OECT is installed on the bottom of the PCB to maintain direct contact with the skin and facilitate attachment to the arm or other body locations using a strap. An Android application was developed to interact with the sensor using an NFC-enabled smartphone, which acts as a reader. The acquired measurements are uploaded to an InfluxDB 2 database and can be viewed through a Grafana web dashboard. Two versions of the app have been developed (see screenshots shown in Fig. 7): one to measure lactate levels in saliva, and another to monitor the lactate concentration produced by athletes' sweat while they exercise. The total board consumption, excluding the OECT current, is typically less than 1.6 mA. Although the electronics can be powered by the energy harvested from the NFC IC when a smartphone is used as a reader, a 1000 mAh Lite-On rechargeable battery can also be used. This is because the measurement time, determined by the sensor's stabilization time, usually lasts several minutes, which is excessive for a user to hold a smartphone over the sensor. The read range with smartphones is typically up to 3 cm. Based on the individual cost of the components and the PCB area, the overall cost of the board is estimated to be less than U.S. $5, depending on the number of units. Therefore, the platform is well-suited for low-cost POCT devices.

IV. Results and Discussion

The validation of the NFC-based measurement platform was achieved by comparing its performance with a reference multimeter. An OECT operating in a 0.1 M PBS solution was

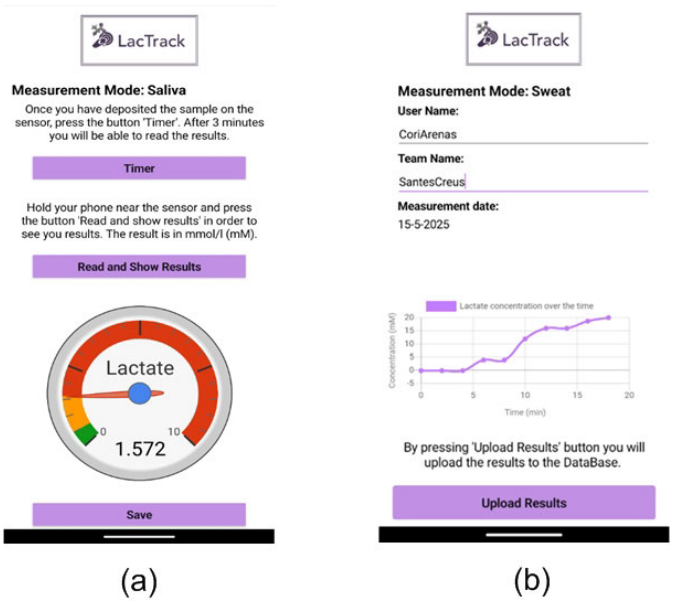


Fig. 7. Screenshots of the app for (a) monitoring saliva and (b) sweat lactate.

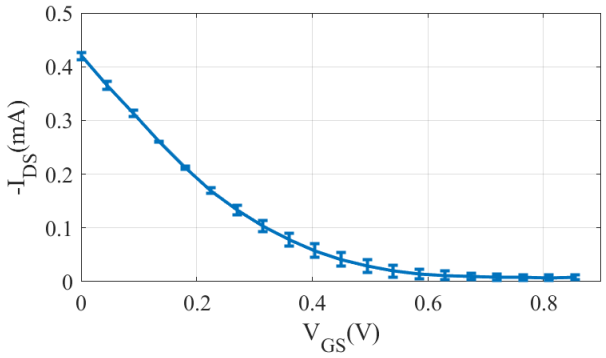


Fig. 8. Measurement of the drain–source current of an OECT in a 0.1 M PBS solution as a function of gate–source voltage V_{GS} for $V_{DS} = -0.5$ V. The error bars show the standard deviation of the error between 5 sweeps measured with the developed board and the values measured with a multimeter used as a reference.

used for the test. The drain-to-source voltage (V_{DS}) was fixed at −0.5 V using the developed board, while a gate-to-source voltage sweep (V_{GS}) from 0 to 0.8 V was programmed. During the measurement, both the channel current (I_{DS}) and the gate-to-source voltage were monitored simultaneously using two Agilent 34450A multimeters, serving as references. Fig. 8 shows the average drain current measured by the developed board. The error bars indicate the standard deviation between the readings obtained from the board and the multimeter in five repeated sweeps. The observed standard deviation, typically in the range of 5–10 μA, is primarily attributed to the variability of the device in the sweeps, rather than being limited by the resolution or noise of the ADC.

The typical composition of human saliva is a complex mixture of water, electrolytes (including sodium, potassium, calcium, magnesium, bicarbonate, and phosphates), mucins, enzymes, antimicrobial agents, and other organic and inorganic compounds [46], [47], [48]. Artificial saliva is commonly used

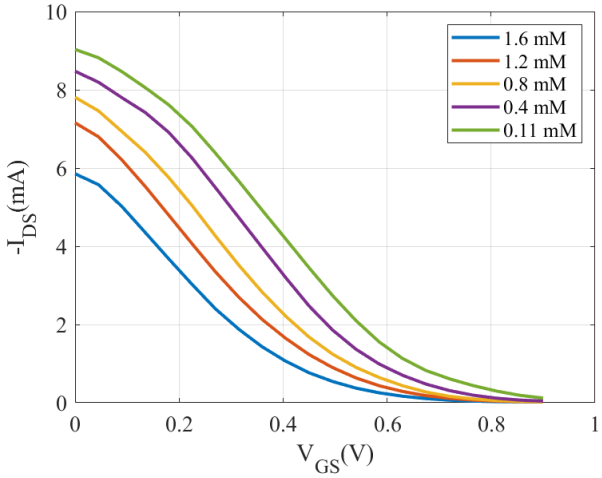


Fig. 9. OECT sensor for detecting lactate in artificial saliva. Measured drain–source current (I_{DS}) as a function of the applied gate voltage (V_{GS}) for different lactate concentrations.

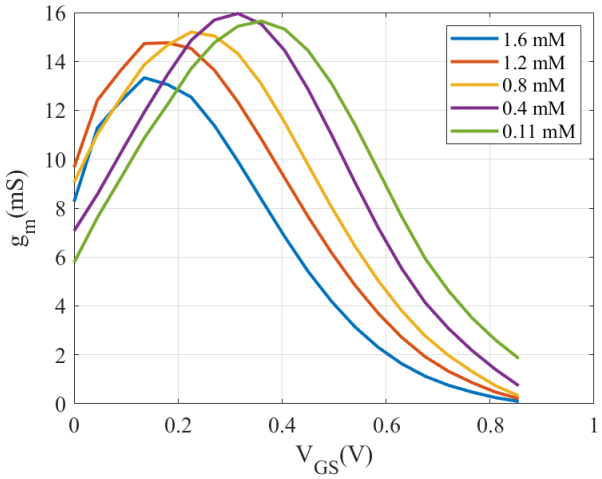


Fig. 10. OECT sensor for detecting lactate in artificial saliva. Measured transconductance (g_m) as a function of the applied gate voltage (V_{GS}) for different lactate concentrations.

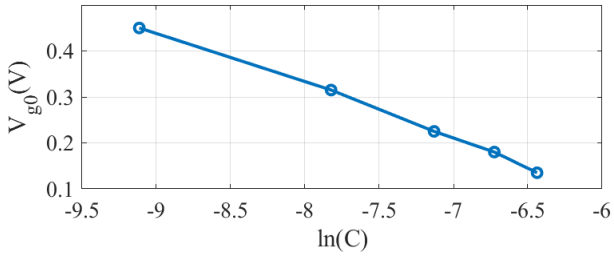


Fig. 11. OECT sensor for detecting lactate in artificial saliva. Measured peak voltage of the transconductance (v_{g0}) as a function of the natural logarithm of the lactate concentration in M.

in studies with a composition similar to human saliva [49], [50]. To evaluate the performance of the saliva lactate sensor, different concentrations of L-lactate (Sigma-Aldrich, reference 7L7022) were prepared in artificial saliva (Sigma-Aldrich, reference SAE0149). The artificial saliva contains 0.126 g of NaCl (2.16 mM), 0.964 g of KCl (12.9 mM), 0.189 g of KSCN (1.95 mM), 0.655 g of KH_2PO_4 (4.81 mM), and 0.200 g of urea (3.3 mM) dissolved in 1 L of deionized water, with a pH of 6.8. In saliva, the concentrations of lactate are much lower than in sweat (5–25 mM) and blood (0.5–15 mM); they range between 0.11 and 0.56 mM under normal conditions and at rest, and can reach up to approximately 1.6 mM at the end of exercise [51]. In diabetic patients, the likelihood of presenting elevated lactate levels is very high due to the intensification of anaerobic glycolysis [52]. Fig. 9 shows the measured drain-to-source current I_{DS} as a function of the gate-to-source V_{GS} in the saturation region ($V_{DS} = -0.5$ V) for different concentrations of lactate in artificial saliva. From these curves, the transconductance (g_m) was calculated by differentiation, yielding the results shown in Fig. 10. The results show a shift in the curves as a function of the Lactate concentration as predicted by theory. A clear peak in the transconductance was obtained for each concentration, which shifts as in the case of the current. Fig. 11 shows the peak voltage of the transconductance as a function of the natural logarithm of lactate concentration in M. This peak indicates the bias point with the highest sensitivity to gate voltage deviations related to concentration changes, as described by (4). A slope of -294 mV/dec has been obtained, demonstrating the high sensitivity of the sensor. Thus, the optimal gate-to-source bias is around 0.3 V.

Fig. 12 shows the chronoamperometry obtained with the OECT sensor after varying the lactate concentration for periods of 100 s. The normalized current variation is used as the calibration curve. To facilitate the comparison between different devices, the normalized response (NR) was calculated relative to the zero concentration limit $I_{DS,conc=0}$ as follows:

$$NR = \frac{I_{DS} - I_{DS,conc=0}}{I_{DS,conc=0}}. \tag{12}$$

The NR of the source–drain current is plotted as a function of lactate concentration in Fig. 13. This result demonstrates that the sensor can be used effectively across a wide range of concentrations (0.1–1.6 mM). A linear trend for the NR is observed on the logarithmic scale within this range, demonstrated by the high correlation coefficient (R = 0.968). The limit of detection (LOD) in an electrochemical sensor refers to the lowest concentration of an analyte that can be reliably distinguished from the background noise. The common method to calculate it is from the slope of the calibration curve or sensitivity (S) and the standard deviation of the noise (blank) σ

$$LOD = \frac{3\sigma}{S}. \tag{13}$$

For the sensor tested in artificial saliva, the LOD obtained was 0.048 mM, which is significantly lower than the typical lactate concentration in human saliva under resting conditions.

Artificial sweat solutions with different concentrations of L-lactate (Sigma-Aldrich, reference 7L7022) have been prepared by dissolving 85 mmol of sodium chloride (NaCl), 13 mmol of potassium chloride (KCl), and 16 mmol of urea (Sigma-Aldrich, reference U5378), in 1 L of distilled

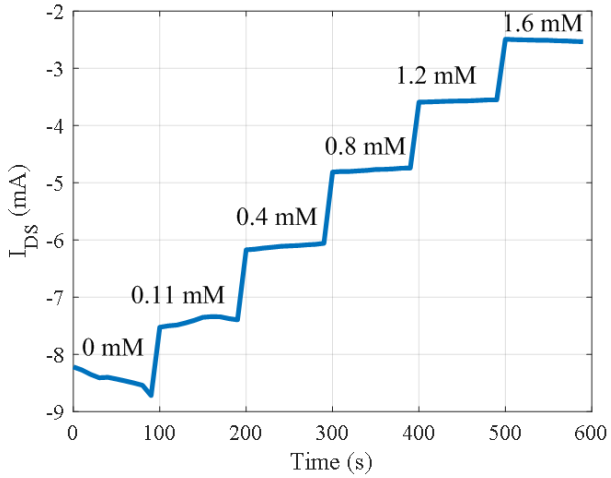


Fig. 12. OECT sensor for lactate detection on artificial saliva. I_{DS} as a function of time for different lactate concentrations ($V_{GS} = 0.3$ V, $V_{DS} = -0.5$ V).

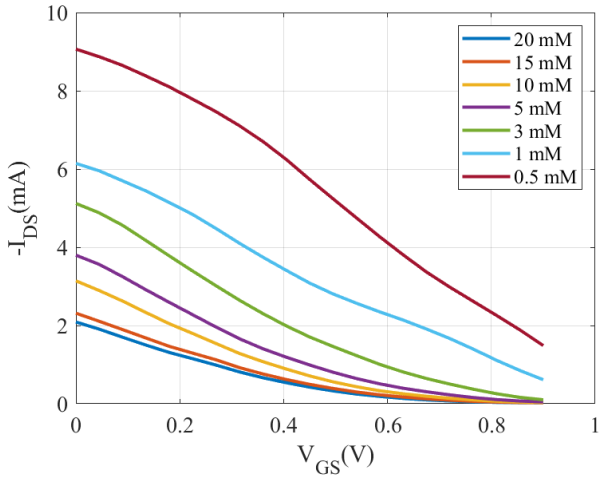


Fig. 14. OECT sensor for lactate detection on artificial sweat. Measured drain–source current (I_{DS}) as a function of applied gate voltage (V_{GS}) for different lactate concentrations.

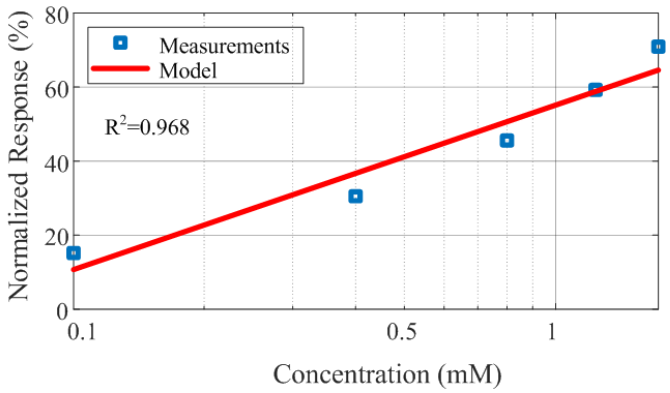


Fig. 13. OECT sensor for lactate detection on artificial saliva. NR as a function of lactate concentrations ($V_{GS} = 0.3$ V, $V_{DS} = -0.5$ V).

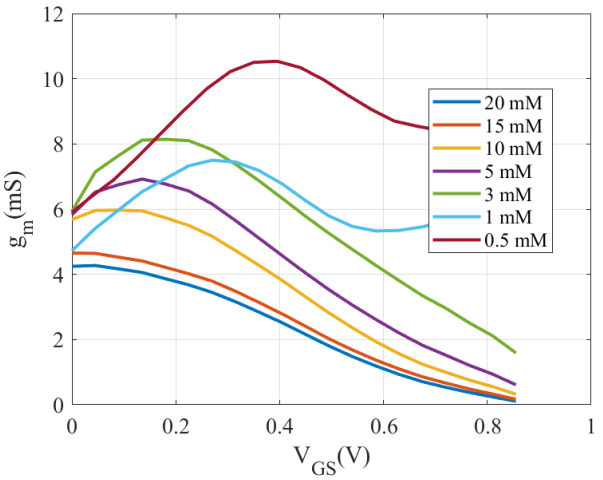


Fig. 15. OECT sensor for lactate detection on artificial sweat. Measured transconductance (g_m) as a function of applied gate voltage (V_{GS}) for different Lactate concentrations.

water [53]. To investigate how the drain current varies with lactate concentration in artificial sweat and determine the optimal bias point, the OECT was characterized across a range of lactate concentrations from 1 to 20 mM. Fig. 14 shows the measured drain current as a function of the gate-to-source voltage. From these curves, the transconductance (g_m) was calculated by differentiation, yielding the results shown in Fig. 15. The results show a shift of the curves as a function of the Lactate concentration as predicted by the theory. A clear peak in the transconductance was obtained for each concentration, which shifts as in the case of the current. Fig. 16 shows the peak voltage of the transconductance achieving an almost linear behavior as a function of the logarithm of the concentration, with a slope of -172 mV/dec.

To obtain a calibration curve, a chronoamperometry measurement was performed with $V_{GS} = 0.3$ V and $V_{DS} = -0.5$ V, varying the lactate concentrations every 100 s. Fig. 17 shows the results, which demonstrate that the sensor can detect lactate concentrations in the typical range of human sweat (1–20 mM). Fig. 18 shows the NR obtained from these measurements and used as a calibration curve.

For the calibration curve, a chronoamperometry measurement is conducted with fixed gate and drain voltages ($V_{GS} = 0.3$ V and $V_{DS} = -0.5$ V). During this process, lactate was introduced at increasing concentrations for periods of 100 s. The data, presented in Fig. 17, clearly indicate the sensor's ability to detect lactate across the typical range observed in human sweat (1–20 mM). The NR derived from these measurements, shown in Fig. 18, was subsequently used as the calibration curve. The NR shows a linear trend on the logarithmic scale within this range, with a high correlation coefficient of $R^2 = 0.997$.

The sensor demonstrated a LOD of 0.36 mM in artificial sweat, which is well below the physiological lactate levels typically observed in resting human sweat. This is higher than that of saliva due to the difference in the electrolytes and pH between the two fluids.

Sensor performance may be affected by the presence of interfering substances. It is known that OECTs with a

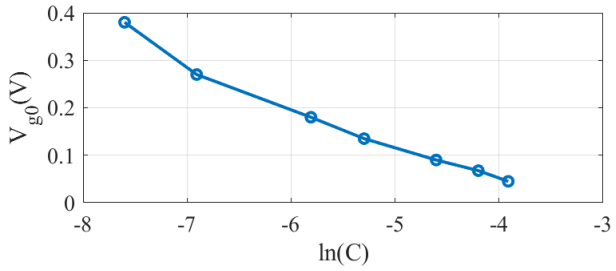


Fig. 16. OECT sensor for lactate detection on artificial sweat. Measured peak voltage of the transconductance (V_{g0}) as a function of the natural logarithm of the lactate concentration in M.

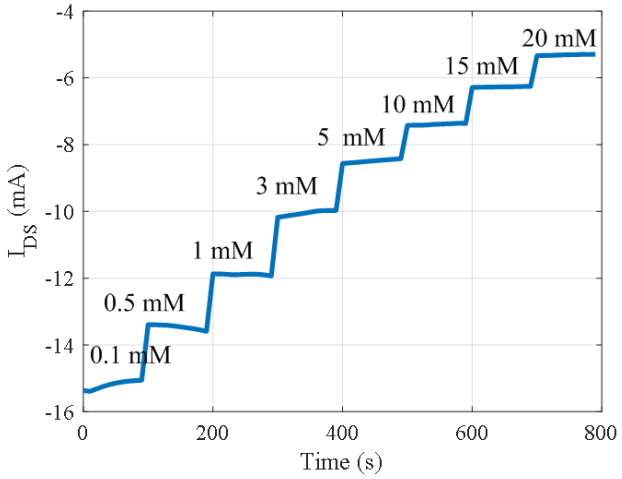


Fig. 17. OECT sensor for lactate detection on artificial sweat. I_{DS} as a function of time for different lactate concentrations (V_{GS} = 0.3V, V_{DS} = −0.5 V).

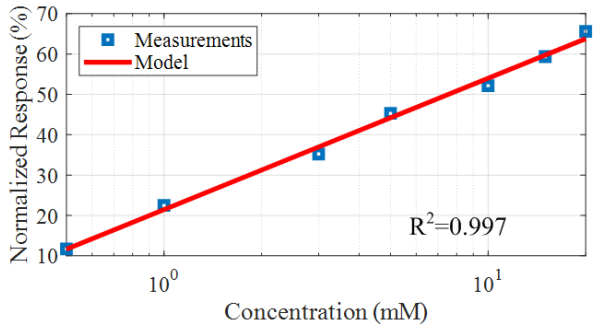


Fig. 18. OECT sensor for lactate detection on artificial sweat. NR as a function of lactate concentrations (V_{GS} = 0.3V, V_{DS} = −0.5V).

non-functionalized gate can respond to species such as UA and ascorbic acid (AA) [54]. The concentration of UA in human sweat is relatively low (25–36 μM) [55] and approximately 30–180 μM in human saliva [56]. The concentration of glucose is typically 0.1–0.6 mM in sweat [12] and around 0.1–0.3 mM in saliva [57].

To investigate the effect of potential interfering substances, chronoamperometry (see Fig. 19) has been performed by modifying a PBS solution containing 4.5 mM lactate with a typical interfering substance composed of: 0.1 mM UA, 0.1 mM AA, 0.25 mM glucose (GLU), and finally 10 mM lactate. The sensor exhibits high specificity for lactate,

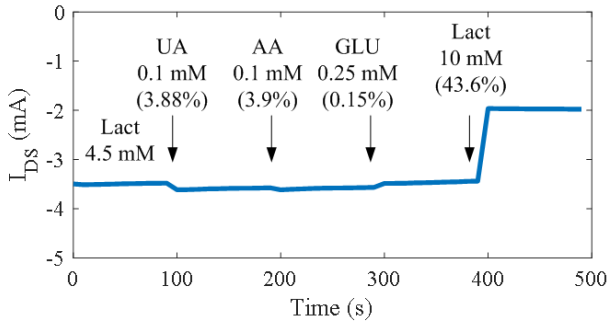


Fig. 19. Response to typical interfering substances. Starting with a PBS solution containing 4.5 mM lactate, potential interfering substances were sequentially added: 0.1 mM UA, 0.1 mM AA, 0.25 mM glucose (GLU), and finally 10 mM lactate. The corresponding relative responses to each substance are presented below by arrows, indicating the moments when each compound was added.

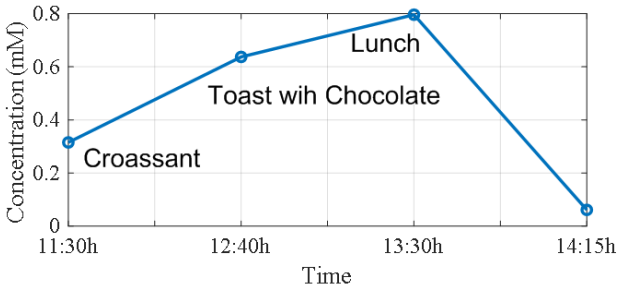


Fig. 20. Concentration of lactate measured in saliva after eating different foods.

evidenced by the notably lower relative response to other substances. This selectivity is primarily attributed to two factors: the highly specific reaction catalyzed by the Lactate Oxidase (LOx) enzyme, which allows targeted detection of lactate over interferents such as glucose, and the enhanced interference rejection provided by the Nafion membrane [58]. As a cation-exchange and anion-repellent material, Nafion permits the selective passage of positively charged species (e.g., protons generated by the LOx reaction, or necessary cations for charge balance) while effectively blocking or significantly reducing the diffusion of negatively charged interfering species such as AA and UA.

Lactate generation after meals, especially those containing carbohydrates (starches, sugars), is a well-known part of metabolism [59], [60]. Fig. 20 shows the results of saliva samples taken from a volunteer after consuming a croissant, two slices of toast with chocolate, immediately following lunch, and 1 h later. The graph demonstrates the capacity of the sensor and the prototype designed to measure variations in human salivary lactate.

The sensor was tested during an outdoor fitness class. It was attached to the arm with a strap. To collect sweat, the active area of the OECT was covered with absorbent filter paper. It took 10 min to generate enough sweat for detection. The sensor measured lactate concentration every 5 min. Simultaneously, heart rate was registered with an Apple Watch. After the session, data were downloaded to a smartphone via NFC using the developed app. Lactate concentration

TABLE I
COMPARISON OF ELECTROCHEMICAL LACTATE BIOSENSORS

Technology	Gate or Working Electrode	Enzyme	Sensing Fluid	Sensitivity	LOD	Range (mM)	Ref.
Electrochemical	Carbon/Nafion/LOx/BSA	LOx	Saliva	21.8 μA/(mMcm^2)	0.25 mM	0.25–1.75	[52]
OECT	Ni/Al LDH	LOx	PBS	22.3 mA/mM	0.04 mM	0.05–8	[62]
OECT	Pt Prussian blue BSA/Chitosan	LOx	PBS	1.9 mA/mM	11 nM	0.25–5	[43]
OECT	Pt/Nafion/LOx/Nafion	LOx	Saliva	3.2 mA/mM	0.045 mM	0.1–2.5	This work
OECT	Pt/Nafion/LOx/Nafion	LOx	Sweat	3.8 mA/mM	0.36 mM	0.5–20	This work

LDH: Layered Double Hydroxide
BSA:Bovine serum albumin

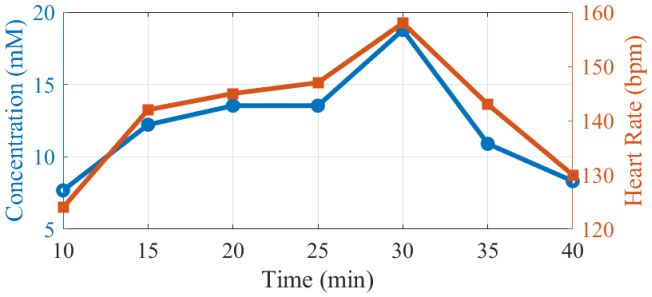


Fig. 21. Concentration of lactate measured in sweat and heart rate in beats per minute as a function of time during physical exercise.

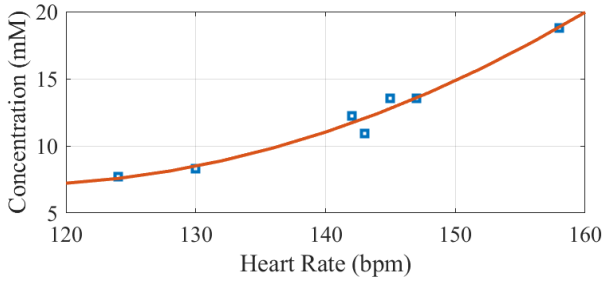


Fig. 22. Concentration of lactate measured in sweat as a function of the heart rate in beats per minute.

increases from approximately 5 mM after 10 min to close to 20 mM after 40 min of exercise. Fig. 21 shows the lactate concentration obtained from the drain current measurement, using the calibration curve for artificial sweat alongside the measured heart rate, which served as an indicator of work effort. Fig. 22 depicts the corresponding lactate concentration as a function of heart rate, showing a parabolic behavior.

The performance of the developed sensor is compared with that of other recent lactate biosensors published in the literature. A comprehensive comparison of electrochemical sensors can be found in [61]. Most of these sensors use lactate oxidase (LOx) as the enzyme, but differ in their working electrodes. The current trend is to incorporate nanomaterials, such as metal oxides and carbon materials, to improve performance. For instance, [52] reports a flexible electrochemical sensor with a LOD of 0.25 mM in saliva (Table I). The detection limit can be improved using Pt gates, as shown in this work, and can be further optimized by incorporating Prussian blue (Ferric ferrocyanide) [43].

In addition to electrochemical sensors, biosensors based on OECTs have been described. Due to the transistor gain, the sensitivity of OECT-based sensors is higher, and the LOD is lower than that of conventional electrochemical ones. Besides the use of Nafion membranes, several methods for immobilizing LOx have been investigated, including the use of bovine serum albumin (BSA) and chitosan [43]. Nafion-based membranes are characterized by their long-term stability and high resistance to interference, making them ideal for robust lactate sensor applications. In contrast, BSA-based membranes offer a simpler, low-cost, and faster fabrication alternative, particularly suitable for laboratory-scale experiments or proof-of-concept studies.

The proposed sensors developed in this work have demonstrated a low LOD and sufficient range for detecting lactate in saliva and sweat. These were fabricated using low-cost standard PCB facilities. Other substrates, such as flexible Kapton, have also been successfully fabricated with similar performance. The thickness of the PEDOT is primarily determined by the thickness of the metallization of the PCB traces. These relatively thick devices result in high-current and high-transconductance devices, which is a key parameter for achieving high sensitivity.

V. CONCLUSION

This study has developed a biosensor system based on OECTs. This system uses NFC for real-time measurement of lactate concentrations in saliva and sweat and is low-cost and low-power. This innovation addresses the critical need for portable and noninvasive lactate monitoring, which has traditionally been limited to high-cost laboratory instruments and blood samples. A negative voltage drain-to-source voltage can be applied to the developed prototype, avoiding the need for dual batteries or noisy inverter-based dc–dc converters. The bias point is accurately set with a potentiostat, and the current is measured using a transimpedance amplifier, which allows low currents to be measured by adjusting the amplifier gain. Therefore, the developed board can be used with other OECT-based sensors, such as a glucose sensor.

The fabricated OECT sensors, which utilize PEDOT:PSS channels and platinum gates functionalized with lactate oxidase (LOx) and Nafion, exhibited excellent sensing capabilities. A microcontroller-based potentiostat, custom-designed to be compatible with single positive voltage sources, enabled efficient polarization and measurement of the OECT drain current. The integration of NFC technology facilitated data retrieval using a smartphone and visualization through a Grafana web dashboard, improving its usefulness for POCT and sports performance monitoring.

Experimental validation in artificial saliva demonstrated the sensor's effectiveness across a physiologically relevant

range of lactate concentrations (0.1–1.6 mM), achieving a low LOD of 0.048 mM. Similarly, tests in artificial sweat confirmed its ability to detect lactate within the typical human sweat range (1–20 mM), with an LOD of 0.36 mM. The observed linear trend in NR on a logarithmic scale, together with high correlation coefficients ($R^2 = 0.968$ for saliva, $R^2 = 0.997$ for sweat), highlights the sensor's robust and predictable performance. Furthermore, initial tests using human saliva samples after carbohydrate intake and physical activity successfully obtained variations in lactate levels, demonstrating the practical applicability of the sensor in everyday scenarios. The relationship between lactate concentration and heart rate during exercise also revealed a parabolic behavior, further validating the sensor's usefulness as a physiological indicator.

There are some future challenges that arise from this work. By resizing the width of the OECT channel, it is possible to reduce the operating current to a value of approximately less than 1 mA, allowing the system to be powered by energy harvesting and thus avoiding the use of batteries. This solution would be particularly interesting in POCT, especially for applications that do not require continuous monitoring. In addition to this reduction in power consumption, response time is a point that can be improved. This can be achieved by reducing the thickness of the membrane and sampling at a fixed time after preparing the sample, similar to the approach used in commercial glucometers based on electrochemical sensors [10].

REFERENCES

[1] E. V. Karpova, A. I. Laptev, E. A. Andreev, E. E. Karyakina, and A. A. Karyakin, "Relationship between sweat and blood lactate levels during exhaustive physical exercise," *ChemElectroChem*, vol. 7, no. 1, pp. 191–194, Jan. 2020.

[2] X. Xuan, C. Pérez-Ràfols, C. Chen, M. Cuartero, and G. A. Crespo, "Lactate biosensing for reliable on-body sweat analysis," *ACS Sensors*, vol. 6, no. 7, pp. 2763–2771, Jul. 2021.

[3] C. A. W. Emhoff et al., "Gluconeogenesis and hepatic glycogenolysis during exercise at the lactate threshold," *J. Appl. Physiol.*, vol. 114, no. 3, pp. 297–306, 2013, doi: 10.1152/japplphysiol.01202.2012.

[4] A. J. Reddy, S. W. Lam, S. R. Bauer, and J. A. Guzman, "Lactic acidosis: Clinical implications and management strategies," *Cleveland Clinic J. Med.*, vol. 82, no. 9, pp. 615–624, Sep. 2015.

[5] J. Chertoff et al., "Lactate kinetics in sepsis and septic shock: A review of the literature and rationale for further research," *J. Intensive Care*, vol. 3, p. 39, 2015, doi: 10.1186/s40560-015-0105-4.

[6] D. Wu et al., "Lactate dehydrogenase a (LDHA)-mediated lactate generation promotes pulmonary vascular remodeling in pulmonary hypertension," *J. Transl. Med.*, vol. 22, p. 738, 2024, doi: 10.1186/s12967-024-05543-7.

[7] P. F. Jorge et al., "The association of early combined lactate and glucose levels with subsequent renal and liver dysfunction and hospital mortality in critically ill patients," *Crit. Care*, vol. 21, p. 218, 2017, doi: 10.1186/s13054-017-1785-z8.

[8] Y. H. Park, D. H. Ryu, B. K. Lee, and D. H. Lee, "The association between the initial lactate level and need for massive transfusion in severe trauma patients with and without traumatic brain injury," *Acute Crit. Care*, vol. 34, no. 4, pp. 255–262, Nov. 2019.

[9] O. Karcioglu, "Diagnostic value of plasma D-lactate level in acute intestinal ischemia," *Int. J. Internal Emergency Med.*, vol. 1, no. 1, p. 1010, 2018.

[10] A. Lazaro, R. Villarino, M. Lazaro, N. Canellas, B. Prieto-Simon, and D. Girbau, "Battery-less NFC potentiostat for electrochemical point-of-care sensors based on COTS components," *Sensors*, vol. 22, no. 19, p. 7213, Sep. 2022. [Online]. Available: https://www.mdpi.com/1424-8220/22/19/7213

[11] Z. Sonner et al., "The microfluidics of the eccrine sweat gland, including biomarker partitioning, transport, and biosensing implications," *Biomicrofluidics*, vol. 9, no. 3, May 2015, Art. no. 031301, doi: 10.1063/1.4921039.

[12] J. Moyer, D. Wilson, I. Finkelshtein, B. Wong, and R. Potts, "Correlation between sweat glucose and blood glucose in subjects with diabetes," *Diabetes Technol. Therapeutics*, vol. 14, no. 5, pp. 398–402, May 2012.

[13] É. Tékus et al., "Comparison of blood and saliva lactate level after maximum intensity exercise," *Acta Biologica Hungarica*, vol. 63, no. 1, pp. 89–98, Mar. 2012.

[14] R. Tiongco, A. Bituin, E. Arceo, N. Rivera, and E. Singian, "Salivary glucose as a non-invasive biomarker of type 2 diabetes mellitus," *J. Clin. Experim. Dentistry*, vol. 10, no. 9, p. e902, 2018.

[15] L. Messina and M. T. Giardi, "Recent status on lactate monitoring in sweat using biosensors: Can this approach be an alternative to blood detection?" *Biosensors*, vol. 15, no. 1, p. 3, Dec. 2024.

[16] L. B. Baker, M. D. Engel, and A. S. Wolfe, "Sweat biomarkers for sports science applications," *Sports Sci. Exch*, vol. 35, pp. 1–9, Jun. 2022.

[17] A. Roda, M. Guardigli, D. Calabria, M. M. Calabretta, L. Cevenini, and E. Michelini, "A 3D-printed device for a smartphone-based chemiluminescence biosensor for lactate in oral fluid and sweat," *Analyst*, vol. 139, no. 24, pp. 6494–6501, 2014, doi: 10.1039/c4an01612b.

[18] R. Beneke, "Lactate threshold concepts: how valid are they?" *Sports Med.*, vol. 33, no. 7, pp. 517–538, 2003.

[19] A. M. Jones, M. Burnley, M. I. Black, D. C. Poole, and A. Vanhatalo, "The maximal metabolic steady state: Redefining the 'Gold standard,'" *Physiol. Rep.*, vol. 7, no. 10, May 2019, Art. no. e14098. [Online]. Available: https://physoc.onlinelibrary.wiley.com/doi/abs/10.14814/phy2.14098

[20] M. Sessolo, J. Rivnay, E. Bandiello, G. G. Malliaras, and H. J. Bolink, "Ion-selective organic electrochemical transistors," *Adv. Mater.*, vol. 26, no. 28, pp. 4803–4807, 2014.

[21] N. Coppedè et al., "Ion selective textile organic electrochemical transistor for wearable sweat monitoring," *Organic Electron.*, vol. 78, Mar. 2020, Art. no. 105579.

[22] D. A. Koutsouras, K. Lieberth, F. Torricelli, P. Gkoupidenis, and P. W. M. Blom, "Selective ion detection with integrated organic electrochemical transistors," *Adv. Mater. Technol.*, vol. 6, no. 12, Dec. 2021, Art. no. 2100591.

[23] Y. Li et al., "Ion-selective organic electrochemical transistors: Recent progress and challenges," *Small*, vol. 18, no. 19, May 2022, Art. no. 2107413.

[24] G. Scheiblin, R. Coppard, R. M. Owens, P. Mailley, and G. G. Malliaras, "Referenceless pH sensor using organic electrochemical transistors," *Adv. Mater. Technol.*, vol. 2, no. 2, Feb. 2017, Art. no. 1600141. [Online]. Available: https://onlinelibrary.wiley.com/doi/abs/10.1002/admt.201600141

[25] A. E. Kirchan, K.-T. Kim, M. K. Steward, and S. Choi, "A PEDOT:PSS-based organic electrochemical transistor with a novel double-in-plane gate electrode for pH sensing application," in *Proc. 19th Int. Conf. Solid-State Sensors, Actuat. Microsyst.*, Jun. 2017, pp. 214–217.

[26] D. A. Bernards, D. J. Macaya, M. Nikolou, J. A. DeFranco, S. Takamatsu, and G. G. Malliaras, "Enzymatic sensing with organic electrochemical transistors," *J. Mater. Chem.*, vol. 18, no. 1, pp. 116–120, 2008.

[27] H. Tang, F. Yan, P. Lin, J. Xu, and H. L. W. Chan, "Highly sensitive glucose biosensors based on organic electrochemical transistors using platinum gate electrodes modified with enzyme and nanomaterials," *Adv. Funct. Mater.*, vol. 21, no. 12, pp. 2264–2272, Jun. 2011.

[28] A. Ait Yazza, P. Blondeau, and F. J. Andrade, "Simple approach for building high transconductance paper-based organic electrochemical transistor (OECT) for chemical sensing," *ACS Appl. Electron. Mater.*, vol. 3, no. 4, pp. 1886–1895, Apr. 2021.

[29] M. Braendlein et al., "Lactate detection in tumor cell cultures using organic transistor circuits," *Adv. Mater.*, vol. 29, no. 13, Apr. 2017, Art. no. 1605744.

[30] I. Gualandi, D. Tonelli, F. Mariani, E. Scavetta, M. Marzocchi, and B. Fraboni, "Selective detection of dopamine with an all PEDOT: PSS organic electrochemical transistor," *Sci. reports*, vol. 6, no. 1, p. 35419, 2016.

[31] D. Arcangeli et al., "Smart bandaid integrated with fully textile OECT for uric acid real-time monitoring in wound exudate," *ACS Sensors*, vol. 8, no. 4, pp. 1593–1608, Apr. 2023.

[32] J. Fan, C. Montemagno, and M. Gupta, "3D printed high transconductance organic electrochemical transistors on flexible substrates," *Organic Electron.*, vol. 73, pp. 122–129, Oct. 2019.

[33] A. Cavallo et al., "Biocompatible organic electrochemical transistor on polymeric scaffold for wound healing monitoring," *Flexible Printed Electron.*, vol. 7, no. 3, Sep. 2022, Art. no. 035009.

[34] I. Gualandi, M. Marzocchi, A. Achilli, D. Cavedale, A. Bonfiglio, and B. Fraboni, "Textile organic electrochemical transistors as a platform for wearable biosensors," *Sci. Rep.*, vol. 6, no. 1, p. 33637, Sep. 2016.

[35] E. Bihar, Y. Deng, T. Miyake, M. Saadaoui, G. G. Malliaras, and M. Rolandi, "A disposable paper breathalyzer with an alcohol sensing organic electrochemical transistor," *Sci. Rep.*, vol. 6, no. 1, p. 27582, Jun. 2016.

[36] L. G. D'Amico et al., "Fully passive electrochemical oxygen sensor enabled with organic electrochemical transistor," *Adv. Mater. Technol.*, vol. 10, no. 10, May 2025, Art. no. 2401875.

[37] M. Caselli et al., "A low power and portable electronic system for a flexible-substrate printed OECT sensor," in *Proc. IEEE Int. Flexible Electron. Technol. Conf. (IFETC)*, Sep. 2024, pp. 1–3.

[38] D. A. Bernards and G. G. Malliaras, "Steady-state and transient behavior of organic electrochemical transistors," *Adv. Funct. Mater.*, vol. 17, no. 17, pp. 3538–3544, Nov. 2007.

[39] B. González, L. Masip, M. Lázaro, R. Villarino, D. Girbau, and A. Lázaro, "A compact DC model for PEDOT-based organic electrochemical transistors (OECTs)," *IEEE Trans. Electron Devices*, vol. 71, no. 11, pp. 6983–6988, Nov. 2024.

[40] B. González and A. Lázaro, "Conductivity-based DC model for OECTs," *IEEE Trans. Electron Devices*, vol. 72, no. 8, pp. 4362–4368, Aug. 2025.

[41] K. Yorita, K. Janko, K. Aki, S. Ghisla, B. A. Palfey, and V. Massey, "On the reaction mechanism of l -lactate oxidase: Quantitative structure-activity analysis of the reaction with para -substituted l -mandelates," *Proc. Nat. Acad. Sci. USA*, vol. 94, no. 18, pp. 9590–9595, Sep. 1997. [Online]. Available: https://www.pnas.org/doi/abs/10.1073/pnas.94.18.9590

[42] I. Leiros et al., "The 2.1 Å structure ofAerococcus viridansL-lactate oxidase (LOX)," *Acta Crystallographica Sect. F Structural Biol. Crystallization Commun.*, vol. 62, no. 12, pp. 1185–1190, Dec. 2006, doi: 10.1107/s1744309106044678.

[43] L. J. Currano, F. C. Sage, M. Hagedon, L. Hamilton, J. Patrone, and K. Gerasopoulos, "Wearable sensor system for detection of lactate in sweat," *Sci. Rep.*, vol. 8, no. 1, p. 15890, Oct. 2018.

[44] F. Salehnia et al., "Battery-free NFC sub-ppm gas sensor for distributed gas monitoring applications at room temperature," *IEEE J. Radio Freq. Identificat.*, vol. 7, pp. 630–643, 2023.

[45] A. Lazaro, R. Villarino, M. Lazaro, N. Canellas, B. Prieto-Simon, and D. Girbau, "Recent advances in batteryless NFC sensors for chemical sensing and biosensing," *Biosensors*, vol. 13, no. 8, p. 775, Jul. 2023. [Online]. Available: https://www.mdpi.com/2079-6374/13/8/775

[46] J. L. Chicharro, A. Lucía, M. Pérez, A. F. Vaquero, and R. Ureña, "Saliva composition and exercise," *Sports Med.*, vol. 26, no. 1, pp. 17–27, Jul. 1998.

[47] H. Ben-Aryeh, M. Cohen, Y. Kanter, R. Szargel, and D. Laufer, "Salivary composition in diabetic patients," *J. Diabetic Complications*, vol. 2, no. 2, pp. 96–99, Apr. 1988. [Online]. Available: https://www.sciencedirect.com/science/article/pii/0891663288900116

[48] P. Ntovas, N. Loumprinis, P. Maniatakos, L. Margaritidi, and C. Rahiotis, "The effects of physical exercise on saliva composition: A comprehensive review," *Dentistry J.*, vol. 10, no. 1, p. 7, Jan. 2022.

[49] J. Pytko-Polonczyk, A. Jakubik, A. Przeklasa-Bierowiec, and B. Muszynska, "Artificial saliva and its use in biological experiments," *J. Physiol. Pharmacol.*, vol. 68, no. 6, pp. 807–813, 2017.

[50] J. Gal, "About a synthetic saliva for in vitro studies," *Talanta*, vol. 53, no. 6, pp. 1103–1115, Mar. 2001. [Online]. Available: https://www.sciencedirect.com/science/article/pii/S0039914000006184

[51] K. Petropoulos, S. Piermarini, S. Bernardini, G. Palleschi, and D. Moscone, "Development of a disposable biosensor for lactate monitoring in saliva," *Sens. Actuators B, Chem.*, vol. 237, pp. 8–15, Dec. 2016.

[52] M. Liu, M. Yang, M. Wang, H. Wang, and J. Cheng, "A flexible dual-analyte electrochemical biosensor for salivary glucose and lactate detection," *Biosensors*, vol. 12, no. 4, p. 210, Mar. 2022.

[53] A. R. Eldamak, S. Thorson, and E. C. Fear, "Study of the dielectric properties of artificial sweat mixtures at microwave frequencies," *Biosensors*, vol. 10, no. 6, p. 62, Jun. 2020. [Online]. Available: https://www.mdpi.com/2079-6374/10/6/62

[54] Z. Xu et al., "A conducting polymer PEDOT: PSS hydrogel based wearable sensor for accurate uric acid detection in human sweat," *Sens. Actuators B, Chem.*, vol. 348, Dec. 2021, Art. no. 130674. [Online]. Available: https://www.sciencedirect.com/science/article/pii/S0925400521012429

[55] C. Moonla, M. I. Khan, S. Akgonullu, T. Saha, and J. Wang, "Touch-based uric acid sweat biosensor towards personal health and nutrition," *Biosensors Bioelectron.*, vol. 277, Jun. 2025, Art. no. 117289. [Online]. Available: https://www.sciencedirect.com/science/article/pii/S0956566325001630

[56] K. Shibasaki, M. Kimura, R. Ikarashi, A. Yamaguchi, and T. Watanabe, "Uric acid concentration in saliva and its changes with the patients receiving treatment for hyperuricemia," *Metabolomics*, vol. 8, no. 3, pp. 484–491, Jun. 2012.

[57] C. Jurysta et al., "Salivary glucose concentration and excretion in normal and diabetic subjects," *BioMed Res. Int.*, vol. 2009, no. 1, Jan. 2009, Art. no. 430426.

[58] M. R. Romero, F. Ahumada, F. Garay, and A. M. Baruzzi, "Amperometric biosensor for direct blood lactate detection," *Anal. Chem.*, vol. 82, no. 13, pp. 5568–5572, Jul. 2010.

[59] J. D. Rabinowitz and S. Enerbäck, "Lactate: The ugly duckling of energy metabolism," *Nature Metabolism*, vol. 2, no. 7, pp. 566–571, Jul. 2020.

[60] R. G. Leija et al., "Enteric and systemic postprandial lactate shuttle phases and dietary carbohydrate carbon flow in humans," *Nature Metabolism*, vol. 6, no. 4, pp. 670–677, Feb. 2024.

[61] Y. Shen et al., "Recent advances in wearable biosensors for non-invasive detection of human lactate," *Biosensors*, vol. 12, no. 12, p. 1164, Dec. 2022.

[62] I. Gualandi et al., "Layered double hydroxide-modified organic electrochemical transistor for glucose and lactate biosensing," *Sensors*, vol. 20, no. 12, p. 3453, Jun. 2020.



Antonio Lazaro (Senior Member, IEEE) was born in Lleida, Spain, in 1971. He received the M.S. and Ph.D. degrees in telecommunication engineering from the Universitat Politecnica de Catalunya (UPC), Barcelona, Spain, in 1994 and 1998, respectively.

He then joined a Faculty Member with UPC, where he currently teaches a course on microwave circuits and antennas. Since July 2004, he has been a Full-Time Professor with the Department of Electronic Engineering, Universitat Rovira i Virgili (URV), Tarragona, Spain. His research interests are microwave device modeling, on-wafer noise measurements, monolithic microwave integrated circuits (MMICs), low phase noise oscillators, MEMS, RFID, UWB, and microwave systems.



Emma Rojas Rodriguez received the dual B.S. degree in biomedical engineering and telecommunications systems and services engineering from Rovira i Virgili University (URV), Tarragona, Spain, in 2025.

She is currently a Research Support Technician with the Department of Electronic, Electrical, and Automatic Engineering, URV, where she started in 2024. Her research interests include the design of innovative sensors, organic electrochemical transistors (OECTs), and embedded systems.



Marc Lazaro was born in Tarragona, Spain, in 1995. He received the B.S. degree in industrial electronics and automation engineering and the M.S. degree in electronic systems engineering and technology (METSE) from Rovira i Virgili University, Tarragona, in 2017 and 2018, respectively, where he is currently pursuing the Ph.D. degree with the Department of Electronics.

Up until now, he has accumulated professional experience as a Data Acquisition Engineer and an Embedded Systems Developer. His research interests include semipassive RFID technologies based on backscattering communication and novel applications based on mmWave identification (MMID).



Ramon Villarino received the B.S. degree in telecommunications technical engineering from Ramon Llull University (URL), Barcelona, Spain, in 1994, and the degree in senior telecommunications engineering and the Ph.D. degree from the Universitat Politecnica de Catalunya (UPC), Barcelona, in 2000 and 2004, respectively.

From 2005 to 2006, he was a Research Associate with the Technological Telecommunications Center of Catalonia (CTTC), Barcelona. He was a Researcher and an Assistant Professor at the Universitat Autònoma de Barcelona (UAB), Barcelona, from 2006 to 2008. Since January 2009, he has been a Full-Time Professor with Universitat Rovira i Virgili (URV), Tarragona, Spain. His research interests include radiometry, microwave devices, and systems based on UWB, RFIDs, and frequency-selective structures using metamaterials (MM).



Benito González was born in Las Palmas de Gran Canaria, Spain, in May 1968. He received the M.S. degree in physics from the University of Santiago de Compostela, Santiago de Compostela, Spain, in 1992, and the Ph.D. degree from the Universidad de Las Palmas de Gran Canaria, Las Palmas de Gran Canaria, in 2001.

From 1996 to 2003, he was an Associate Professor with the Universidad de Las Palmas de Gran Canaria, where he has been a Faculty Member, since then. His research interests include semiconductor device physics, modeling, characterization, and simulation, with emphasis on self-heating effects.



David Girbau (Senior Member, IEEE) received the B.Sc. degree in telecommunication engineering, the master's degree in electronics engineering, and the Ph.D. degree in telecommunication from Universitat Politecnica de Catalunya (UPC), Barcelona, Spain, in 1998, 2002, and 2006, respectively.

From February 2001 to September 2007, he was a Research Assistant at UPC. From September 2005 to 2007, he was a Part-Time Assistant Professor at Universitat Autònoma de Barcelona (UAB), Barcelona. Since October 2007, he has been a Full-Time Professor with Universitat Rovira i Virgili (URV), Tarragona, Spain. His research interests include microwave devices and systems, with an emphasis on UWB, RFIDs, RF-MEMS, and wireless sensors.